A&A 525, A120 (2011)
DOI: 10.1051/0004-6361/201015235
© ESO 2010

Astronomy & Astrophysics

VLA observations of water masers towards 6.7 GHz methanol maser sources

A. Bartkiewicz[1], M. Szymczak[1], Y. M. Pihlström[2,3], H. J. van Langevelde[4,5], A. Brunthaler[6], and M. J. Reid[7]

[1] Toruń Centre for Astronomy, Nicolaus Copernicus University, Gagarina 11, 87-100 Toruń, Poland
e-mail: annan@astro.uni.torun.pl
[2] Department of Physics and Astronomy, MSC07 4220, University of New Mexico, Albuquerque, NM 87131, USA
[3] National Radio Astronomy Observatory, 1003 Lopezville Road, Socorro, NM 87801, USA
[4] Joint Institute for VLBI in Europe, Postbus 2, 7990 AA Dwingeloo, The Netherlands
[5] Sterrewacht Leiden, Leiden University, Postbus 9513, 2300 RA Leiden, The Netherlands
[6] Max-Planck-Insitut für Radioastronomie, Auf dem Hügel 69, 53121 Bonn, Germany
[7] Harvard-Smithsonian Center for Astrophysics, 60 Garden Street, Cambridge, MA 02138, USA

Received 18 June 2010 / Accepted 9 September 2010

ABSTRACT

Context. Both 22 GHz water and 6.7 GHz methanol masers are usually interpreted as signposts of early stages of high-mass star formation but little is known about their associations and the physical environments in which they occur.
Aims. We attempt to derive accurate positions and morphologies of the water maser emission and relate them to the methanol maser emission mapped earlier with Very Long Baseline Interferometry.
Methods. We searched for 22 GHz water masers in 31 methanol maser sources was searched for 22 GHz water masers using the VLA and observed in the 6.7 GHz methanol maser line with the 32 m Torun dish simultaneously.
Results. Water maser clusters are detected towards 27 sites leading to the identification of 15 new sources. The detection rate of water maser emission associated with methanol sources is as high as 71%. In a large number of objects (18/21), the structure of water maser is well aligned with that of the extended emission at 4.5 μm confirming the origin of water emission in outflows. The sources of methanol emission with ring-like morphologies, which likely trace a circumstellar disc/torus, either do not show associated water masers or the distribution of water maser spots is orthogonal to the major axis of the ring.
Conclusions. The two maser species are generally powered by the same high-mass young stellar object but probe different parts of its environment. The morphology of water and methanol maser emission in a minority of sources is consistent with a scenario where 6.7 GHz methanol masers trace a disc/torus around a protostar while the associated 22 GHz water masers arise in outflows. The majority of sources in which methanol maser emission is associated with the water maser appear to trace outflows. The two types of associations may be related to different evolutionary phases.

Key words. stars: formation – ISM: molecules – masers – techniques: interferometric

1. Introduction

Studies of high-mass star-forming regions (HMSFRs) are difficult but important in astrophysics as these regions are responsible for much of the energetic phenomena we see in galaxies. However, their large distances, heavy obscuration, and rapid evolution make observations challenging. Maser emission has become a unique tool for studying massive star formation. Methanol masers at 6.7 GHz as well as water masers at 22 GHz have been recognized as tracers of massive star formation (e.g., Caswell et al. 1995; Menten 1991; Sridharan et al. 2002; Urquhart et al. 2009). Moreover, both maser species have been found to be associated with the very early stages of a protostar, when it still accretes and before it begins to ionise the surrounding medium. These masers are often detectable before an ultra-compact H II region is seen at cm wavelengths.

Studies of maser emission on the milliarcsecond scale, using Very Long Baseline Interferometry (VLBI) techniques, have detected a wide range of morphologies for 6.7 GHz methanol masers. They can form simple structures (a single spot), lie in linear structures or arcs, or be distributed randomly without any apparent regularity (e.g., Minier et al. 2000; Norris et al. 1998; Phillips et al. 1998; Walsh et al. 1998). However, it is still unclear where and how they are produced. *Are they related to discs/tori around young massive protostars or found in outflows or shocks?* (e.g., Dodson et al. 2004; Minier et al. 2000; Walsh et al. 1998). Detailed studies of particular sources provide additional clues about the origin of methanol masers. Unfortunately, they are not always consistent with one scenario. High angular resolution mid-infrared (MIR) observations by De Buizer & Minier (2005) indicated that the outflow scenario is more plausible in the case of NGC 7538 IRS 1, where the linear structure of methanol masers had been proposed to originate in an edge-on Keplerian disc (Pestalozzi et al. 2004). On the other hand, van der Walt et al. (2007) argued that a simple Keplerian-like disc model was more consistent with the observed kinematics of methanol maser spots in linear structures than the shock model proposed by Dodson et al. (2004).

A relatively high detection rate of water masers towards methanol masers is confirmed with single-dish studies. Szymczak et al. (2005) observed 79 targets with 6.7 GHz methanol maser emission and detected the 22 GHz water line in 52% of cases. Sridharan et al. (2002) also reported a detection rate of 42% for 69 HMSFRs. In interferometric investigations,

Table 1. 6.7 GHz methanol maser sites searched for the 22 GHz water maser emission.

Source*	Position of 6.7 GHz masers		V_p	Secondary calibrator	Synthesized beam	rms noise
Gll.lll±bb.bbb	RA(h m s)	Dec(° ′ ″)	(km s^{-1})	calibrator	maj, min; PA (″, ″;°)	per channel (mJy beam^{-1})
G21.407−00.254	18 31 06.33794	−10 21 37.4108	89.0	J1832−1035	1.19, 0.49;+61	2
G22.335−00.155	18 32 29.40704	−09 29 29.6840	35.6	J1832−1035	1.07, 0.72;+48	4
G22.357+00.066	18 31 44.12055	−09 22 12.3129	79.7	J1832−1035	1.36, 0.73;+39	3
G23.207−00.377	18 34 55.21212	−08 49 14.8926	77.1	J1832−1035	1.05, 0.85;+2	4
G23.389+00.185	18 33 14.32477	−08 23 57.4723	75.4	J1832−1035	0.88, 0.84;+83	3
G23.657−00.127	18 34 51.56482	−08 18 21.3045	82.6	J1832−1035	1.03, 0.55;−77.5	3
G23.707−00.198	18 35 12.36600	−08 17 39.3577	79.2	J1832−1035	1.22, 0.84;−37	4
G23.966−00.109	18 35 22.21469	−08 01 22.4698	70.9	J1832−1035	1.70, 0.72;−44	5
G24.148−00.009	18 35 20.94266	−07 48 55.6745	17.8	J1832−1035	1.65, 0.52;−60	4
G24.541+00.312	18 34 55.72152	−07 19 06.6504	105.7	J1832−1035	1.89, 0.74;−48	6
G24.634−00.324	18 37 22.71271	−07 31 42.1439	35.4	J1832−1035	2.82, 0.60;+42	3
G25.411+00.105	18 37 16.92106	−06 38 30.5017	97.3	J1832−1035	0.35, 0.35;+45	3
G26.598−00.024	18 39 55.92567	−05 38 44.6424	24.2	J1832−1035	3.38, 0.65;−46	3
G27.221+00.136	18 40 30.54608	−05 01 05.3947	118.8	J1832−1035	1.20, 0.89;+47	5
G28.817+00.365	18 42 37.34797	−03 29 40.9216	90.7	J1851+0035	4.56, 0.62;+41	4
G30.318+00.070	18 46 25.02621	−02 17 40.7539	36.1	J1851+0035	1.48, 0.71;+38	3
G30.400−00.296	18 47 52.29976	−02 23 16.0539	98.5	J1851+0035	1.36, 0.64;+45	4
G31.047+00.356	18 46 43.85506	−01 30 54.1551	80.7	J1851+0035	1.02, 0.82;+44	3
G31.581+00.077	18 48 41.94108	−01 10 02.5281	95.6	J1851+0035	0.96, 0.88;+50	2
G32.992+00.034	18 51 25.58288	+00 04 08.3330	91.8	J1851+0035	0.92, 0.82;−39	3
G33.641−00.228	18 53 32.563	+00 31 39.180	58.8	J1851+0035	1.01, 0.83;−57	5
G33.980−00.019	18 53 25.01833	+00 55 25.9760	58.9	J1851+0035	1.03, 0.80;−58	4
G34.751−00.093	18 55 05.22296	+01 34 36.2612	52.7	J1851+0035	1.02, 0.81;−60	5
G35.793−00.175	18 57 16.894	+02 27 57.910	60.7	J1851+0035	1.15, 0.80;−53	4
G36.115+00.552	18 55 16.79345	+03 05 05.4140	73.0	J1851+0035	1.46, 0.70;−51	5
G36.705+00.096	18 57 59.12288	+03 24 06.1124	53.1	J1851+0035	2.09, 0.65;−48	3
G37.030−00.039	18 59 03.64233	+03 37 45.0861	78.6	J1851+0035	2.05, 0.72;+42	6
G37.598+00.425	18 58 26.79772	+04 20 45.4570	85.8	J1851+0035	2.36, 0.64;+42	6
G38.038−00.300	19 01 50.46947	+04 24 18.9559	55.7	J1851+0035	2.74, 0.65;−48	5
G38.203−00.067	19 01 18.73235	+04 39 34.2938	79.6	J1851+0035	2.11, 0.78;−47	10
G39.100+00.491	19 00 58.04036	+05 42 43.9214	15.3	J1851+0035	2.24, 0.77;−46	11

Notes. * The Galactic coordinates of the brightest 6.7 GHz methanol maser spots (Bartkiewicz et al. 2009).

Beuther et al. (2002) achieved a 62% detection rate of water masers towards methanol masers. Breen et al. (2010) observed 379 water masers and detected methanol emission in ≈52% of the sources. Although different excitation conditions are required for both molecules, their origin is quite closely related to the same powering source.

The methanol-water maser associations of few HMSFRs have been studied in detail. For example, Pillai et al. (2006) observed the HMSFR G11.11−0.12 over a wide wavelength range. They reported that methanol masers were associated with an accretion disc driving an outflow traced by water maser emission. Moscadelli et al. (2007) explored HMSFR G24.78+0.08 and showed that water masers trace a rapidly expanding shell closely surrounding a hyper-compact H II region. Methanol masers were proposed to have emerged from a rotating toroid aligned radially outwards of the H II region. However, there is a lack of data for a large sample of methanol and water masers at high angular resolution with a low mJy sensitivity to get better statistics on the two types of associations.

We completed a survey of 31 sources at 6.7 GHz using the European VLBI Network (EVN) (Bartkiewicz et al. 2009). Owing to the high angular and spectral resolution as well as the high sensitivity of our survey, we discovered nine sources (29% of the sample) with ring-like maser distributions (with a typical major axis of 0.″19). These ring-like structures are strongly consistent with a central object hypothesis, and could provide a clue to its nature. Each source with ring-like morphology coincides to within 1″ with a MIR object (from the GLIMPSE survey) that has an excess of 4.5 μm emission, which is evidence of shocked regions (e.g., Cyganowski et al. 2008). This suggests that even ring-like structures can be produced by either shock waves or outflows. To answer the question *what are these structures?*, we initiated wide and detailed studies of that sample of methanol maser sources. Here, we present the first results of our investigation of the presence, position, and distribution of water maser emission towards 6.7 GHz methanol maser emission. We used the NRAO Very Large Array (VLA) to search for water masers near the locations of 6.7 GHz methanol masers and, if detected, to compare the positions of the two masing species.

2. Observations and data reduction

2.1. VLA observations

To investigate the relationship between water and methanol masers in HMSFRs, our sample of 31 methanol maser sources (Table 1) was observed at 22.23508 GHz using the VLA in CnB configuration in two 12 h runs on 2009 June 4 and 5 (the project

Table 2. Results of H_2O observations.

Gll.lll±bb.bbb	RA(J2000) (h m s)	Dec(J2000) (°′″)	V_p (km s^{-1})	ΔV (km s^{-1})	S_p (Jy b^{-1})	S_{int} (Jy km s^{-1})	Δ_{wm} (″)	Δ_{wm} (km s^{-1})	PA_{H_2O} (°)	PA_{MIR} (°)
G21.407−00.254[2]	18 31 06.3380	−10 21 37.460	92.9	7.9	0.68	1.57	0.03	2.2	−27	*−30*
G22.335−00.155[2]	18 32 29.4070	−09 29 29.734	29.0	7.2	0.76	1.12	0.01	−2.6	12	22
G22.357+00.066	18 31 44.1210	−09 22 12.362	88.3	30.2	3.14	7.75	0.04	1.5	−29	8
G23.207−00.377	18 34 55.2019	−08 49 14.943	73.2	29.0	11.46	55.8	0.06	1.2	57	*52*
G23.389+00.185	18 33 14.3250	−08 23 57.522	78.0	2.6	0.15	0.28	0.03	−0.9	90	*−80*
G23.657−00.127					<0.015					
G23.707−00.198[2]	18 35 12.4165	−08 17 39.108	72.6	13.8	0.91	0.57	0.77	−1.3	64	*−69*
G23.966−00.109	18 35 22.2150	−08 01 22.520	48.9	42.7	1.12	5.98	0.03	1.8	−13	−12
G24.155−00.010[1,2]	18 35 21.9019	−07 48 34.575	24.4	24.4	0.17	0.20	25.5	5.3		
G24.534+00.319[1]	18 34 53.4636	−07 19 19.000	101.1	2.0	0.19	0.18	35.8	−2.7		
G24.634−00.324					<0.015					
G25.411+00.105					<0.015					
G26.598−00.024	18 39 55.9561	−05 38 44.692	22.2	7.3	1.09	0.54	0.14	−3.7	−76	−71
G27.221+00.136					<0.025					
G28.817+00.365	18 42 37.2368	−03 29 41.121	88.1	66.5	13.07	34.76	0.37	−2.7	−89	−88
G30.318+00.070	18 46 25.0260	−02 17 40.954	49.9	20.4	2.81	9.99	0.20	−4.2	−56	*−67*
G30.403−00.297[1,2]	18 47 52.9295	−02 23 11.303	125.5	7.9	0.08	0.17	10.5	19.8		
G31.047+00.357[1,2]	18 46 43.5549	−01 30 52.855	77.4	27.0	0.67	1.89	4.64	14.8		
G31.581+00.077[2]	18 48 41.9510	−01 10 02.578	99.5	13.8	12.55	2.22	0.11	1.8	−53	−60
G32.992+00.034[2]	18 51 25.5820	+00 04 07.233	76.0	20.4	1.61	0.54	1.06	−3.8	90	*−66*
G33.641−00.228	18 53 32.5630	+00 31 39.130	56.8	30.9	5.12	15.4	0.10	0.7	0	18
G33.980−00.019[2]	18 53 25.0180	+00 55 26.076	62.2	3.3	0.40	0.49	0.25	2.6	1	5
G34.751−00.093[2]	18 55 05.2220	+01 34 36.361	52.7	36.8	0.53	2.51	0.10	−4.6	27	26
G35.793−00.175[2]	18 57 16.8840	+02 27 57.950	58.7	15.1	2.39	3.53	0.16	1.3	35	36
G36.115+00.552	18 55 16.7830	+03 05 05.514	78.3	39.5	4.91	10.24	0.09	−2.1	57	*72*
G36.705+00.096[2]	18 57 59.1320	+03 24 06.062	56.4	12.5	0.55	0.71	0.15	0.9	−64	−80
G37.030−00.039[2]	18 59 03.6420	+03 37 45.086	81.2	10.5	0.27	0.78	0.01	−1.3		
G37.598+00.425	18 58 26.7970	+04 20 45.407	100.9	40.2	2.91	11.69	0.05	13.9	42	*39*
G38.041−00.298[1,2]	19 01 50.4088	+04 24 32.705	62.3	17.8	0.15	0.28	13.8	2.6		
G38.203−00.067[2]	19 01 18.7320	+04 39 34.243	90.1	11.9	0.63	1.54	0.05	0.7	−45	*−35*
G39.100+00.491	19 00 58.0601	+05 42 44.321	23.9	2.0	0.64	1.32	0.35	8.6	−48	−41

Notes. [1] The position of the H_2O maser differs by more than 3.″6 from that of CH_3OH maser (Bartkiewicz et al. 2009) and its name is updated. [2] New detection.

AB1324). A spectral line mode with a single IF and 6.25 MHz bandwidth divided into 128 spectral channels was used, yielding a velocity coverage of 84 km s^{-1} and a channel spacing of 0.65 km s^{-1}. The pointing positions were defined as the coordinates of the brightest 6.7 GHz methanol maser component (Table 1) and the bandpass was centred on the methanol maser peak velocity taken from Bartkiewicz et al. (2009, their Table 5). 3C 286 was used as the primary flux density calibrator for all targets. We used two secondary calibrators (J1851+0035 and J1832−1035) to monitor changes in interferometer amplitude and phase; these were selected from the VLA calibrator catalog to be near the targets (Table 1). We allocated 50 s to observe the secondary calibrator, followed by 250 s for the maser source. These times included slew and on-source integration times. In total, each target was observed for 35 min, resulting in about 29 min of on-source integration time.

The data reduction was carried out following the standard recipes recommended in Appendix B of the AIPS cookbook[1]. The amplitude and phase errors of 3C 286 were corrected using the default source model and 3C 286 was subsequently used to derive the secondary-calibrator flux densities. The antenna gains were calibrated using the secondary-calibrator data. A few bad data points were flagged and images (512 × 512 pixels with pixel size of 0.″15) were created using natural weighting. The noise levels in the maps and the synthesized beams are listed in Table 1. The analysis of maser properties was carried out using maps centred on the position of the brightest water maser spots.

We estimate that, with the relatively stable weather conditions during our observations, position errors of water maser spots are dominated by the errors in the secondary-calibrator positions, which could be as large as 0.″15 for these two calibrators. However, the relative position uncertainties are much smaller (≈10 mas).

2.2. 32 m dish observations

The same sample was observed in the 6.7 GHz methanol maser line using the Torun 32 m telescope over 20 days in June 2009 nearly simultaneously with the VLA H_2O observations. The telescope characteristics and calibration procedures were described in Szymczak et al. (2002). The spectra were taken in frequency switching mode with a resulting spectral channel spacing

[1] See http://www.nrao.edu/aips/cookbook.html

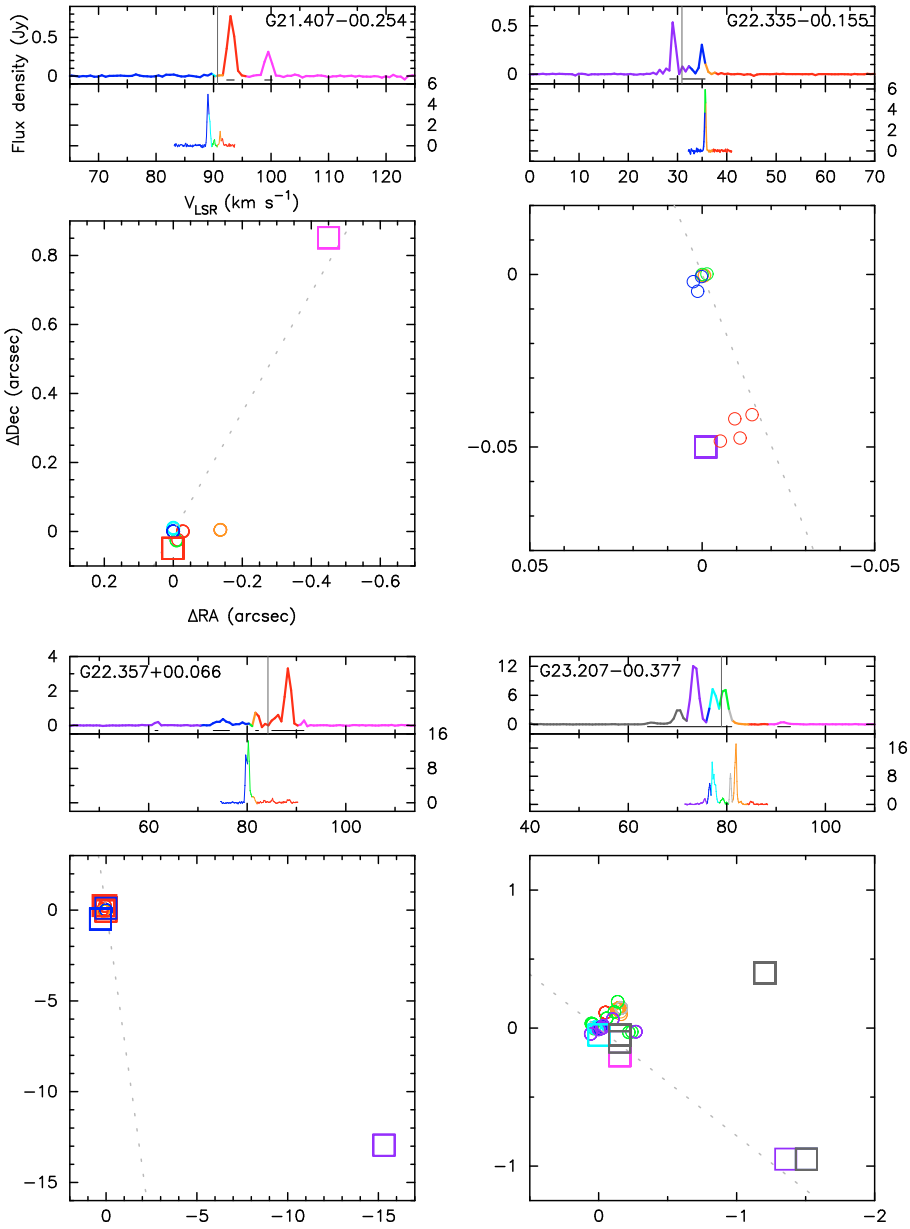

Fig. 1. Spectra and maps of the 22 GHz water (VLA) and 6.7 GHz methanol (EVN) maser emission. *The upper and lower panels* correspond to the water and methanol maser spectra, respectively. The thin bars under the spectra show the velocity ranges of the displayed water maser spots. The thin grey lines represent the systemic velocities of sources (Table 4). Each square represents a 22 GHz water maser spot observed in a single channel. Note that the typical absolute positional uncertainty of water emission is 0.″15. The circles represent the 6.7 GHz methanol maser spots from Bartkiewicz et al. (2009) with the absolute positional accuracy of a few mas. The colours of squares and circles relate to the LSR velocities as indicated in the spectra. The coordinates are relative to the brightest spots of *methanol* emission (Table 1). Note that the source names are the Galactic coordinates of the brightest spot of the *methanol* maser. The dotted lines correspond to the PA_{MIR} of 4.5 μm counterparts as listed in Table 2. *The colour version is available on-line.*

of 0.04 km s^{-1} and sensitivity of ~0.6 Jy (3σ). The accuracy of the absolute flux density calibration was superior to 15%.

3. Results

The observational results are summarized in Table 2 and Fig. 1. Table 2 lists the coordinates of the brightest water maser spot in each target, the LSR velocity (V_p), and the intensity (S_p) as well as both the velocity extent of the water emission (ΔV) and the integrated flux density (S_{int}). In most cases, the Galactic names of the water maser sources are the same as those of the methanol masers in Bartkiewicz et al. (2009). However, for five water maser sources the names are updated (marked by [1]) as their positions differ by more than 3.″6 (0.″001) from the methanol maser positions. The two columns of Table 2, Δ_{wm}, indicate the angular separation of the two nearest spots of both species and the corresponding difference in velocity. The last two columns, PA_{H_2O} and PA_{MIR}, list the position angles of both the water maser emission and the MIR counterpart if it exists (Sect. 3.3). The PA is defined as east of north in the throughout paper.

In Fig. 1, we present the spectra and angular distributions of the water maser emission for the detected sources. The spectra were extracted from the map data cubes using the AIPS task ISPEC and represent the total flux density of maser emission measured in the maps. All spots detected in each of the individual channel maps are shown. Overlaid are the spectra and distributions of the 6.7 GHz methanol masers obtained with the EVN (Bartkiewicz et al. 2009). The parameters of all detected water maser spots of each source are listed in Table 3, i.e., the position (ΔRA, ΔDec) relative to the brightest 6.7 GHz *methanol* maser spot (as listed in Table 1), the LSR velocity (V_{LSR}), and the intensity (S) of the maser spots.

Owing to the relatively poor spectral resolution of 0.65 km s^{-1} of our water maser spectra, we postpone an analysis of line profiles until follow-up VLBI observations of a higher spectral resolution will be acquired.

3.1. Association of water and methanol masers

In the VLA cubes of size 77″ × 77″, water masers were detected in 27 out of 31 cases, out of which 15 are new detections.

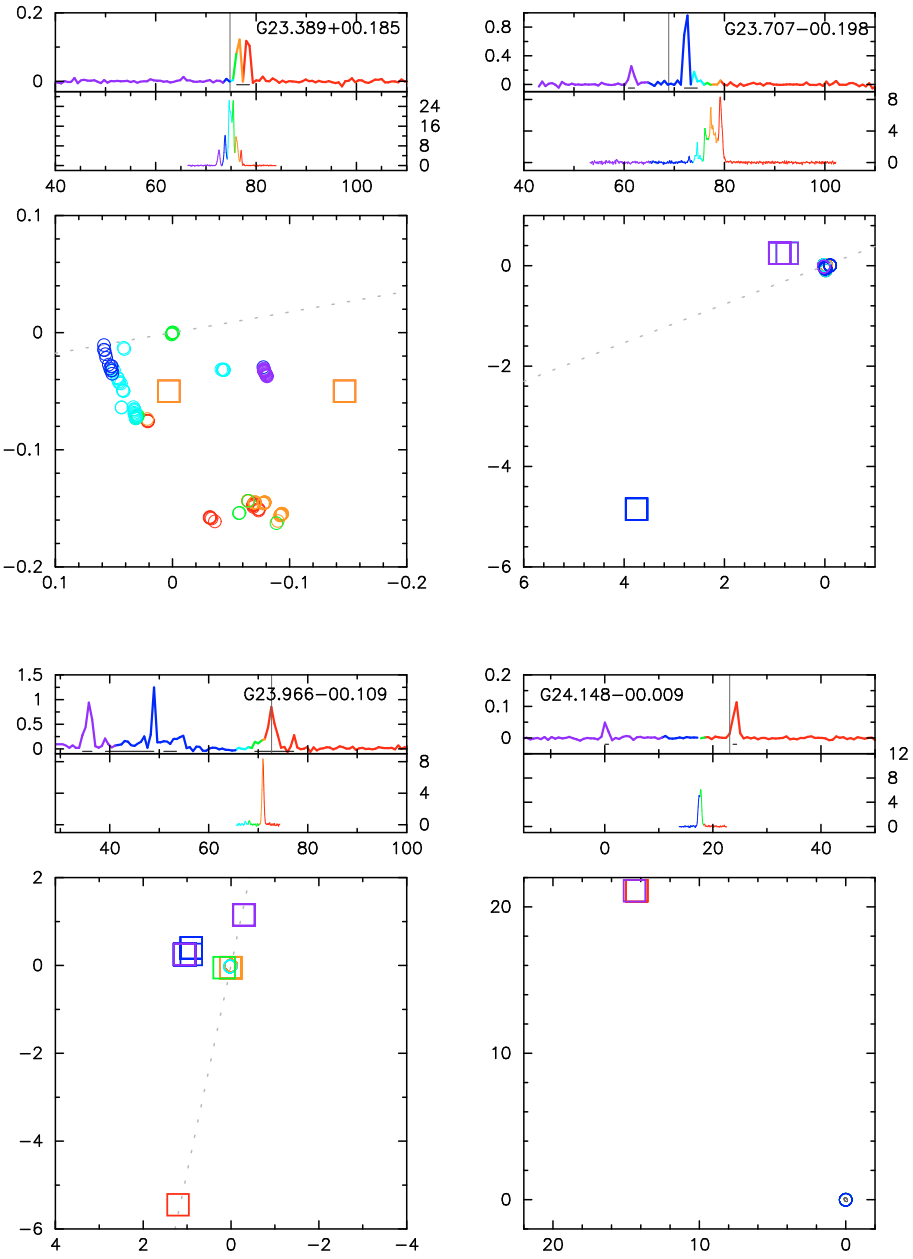

Fig. 1. continued. The radio continuum emission at the level of $3\sigma_{\rm rms}$ detected towards G24.148−00.009 is also indicated by a black contour (Bartkiewicz et al. 2009).

A total of 339 distinct maser spots were detected. To define the detection rate of water masers actually associated with the methanol masers, we need to determine their relative separation in physical coordinates. The near-far distance ambiguity is not clearly resolved for our sources, but it has been argued that the near kinematic distances are more likely (Szymczak et al. 2005). Measurements of the trigonometric parallaxes of several methanol sources (Reid et al. 2009; Rygl et al. 2010) strongly support this assumption. In the following, we therefore use only the near kinematic distance estimates, calculated following the prescription given by Reid et al. (2009). The systemic velocities, $V_{\rm sys}$, were taken from either the observations of optically thin thermal lines (Szymczak et al. 2007) or the mid-range velocity of methanol maser features (Bartkiewicz et al. 2009). The projected linear separations, $\Delta_{\rm wm_{dist}}$ (pc), between the nearest spots of the water and methanol emission were then calculated using the angular separation from Table 2. The near kinematic distances for all 31 objects and the linear separations are listed in Table 4.

For the majority of the detections (22 of 27), the methanol emission is displaced by less than 0.026 pc with a median value of 0.0017 pc (Table 4, Fig. 2). In these sources, the velocity difference between the nearest spots of both masers ranges from 0.7 to 13.9 km s^{-1}, with a median value of 1.95 km s^{-1}. The intrinsic separation of the water and methanol spots may be slightly different because the position uncertainty of 0.″15 results in 0.002−0.005 pc displacement for our sources and there is likely an additional spatial offset along the line of sight that is not accounted for using only the projected separation. It is remarkable that the largest linear separation of 0.026 pc, for the objects considered to have associated methanol and water masers, is consistent with the mean separation of ∼0.03 pc between the stellar objects observed in the Orion Nebula Cluster (McCaughrean & Stauffer 1994), while the median separation of 0.0017 pc agrees well with the mean separation of 0.002 pc between protostellar objects predicted by the merging model of massive star formation (Stahler et al. 2000). The results imply that the water and

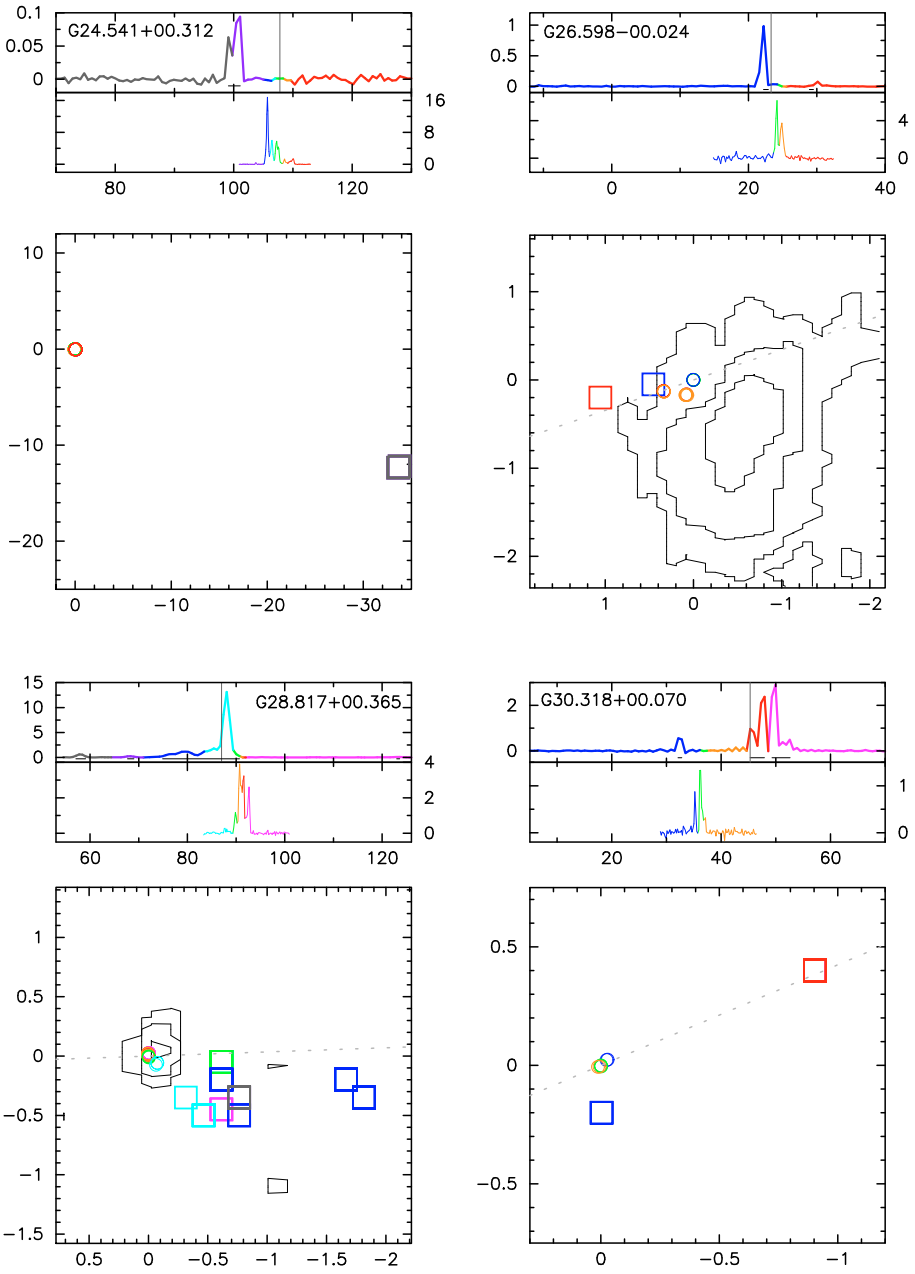

Fig. 1. continued. The radio continuum emission at the levels of 3, 10 and 30 × $\sigma_{\rm rms}$ detected towards G26.598−00.024 and G28.817+00.365 are indicated by black contour lines (Bartkiewicz et al. 2009).

methanol masing regions are associated with the same protostellar object in 22 sources. The emissions of the two maser species for the remaining five sources are separated by >0.1 pc (see Table 4, Fig. 2), which implies that the two species are associated with different young stellar objects within these clusters.

We conclude that at least 71% (22/31) of the methanol maser sources in the sample have associated water masers. This may indicate that both maser species are excited by the same underlying central object or closely associated objects. This detection rate is higher than the 52% inferred from the 100 m dish observation of a much larger sample (Szymczak et al. 2005). However, we note that the 100 m dish survey was about 60 times less sensitive than the VLA observations. We achieve a detection rate of 55% for the VLA data above a flux of 0.45 Jy (the mean rms noise value of observations using the Effelsberg antenna). Our analysis finds that both methanol and water masers are associated with the same underlying object or closely projected objects, implying that the two maser species share a common stage in the early evolution of massive star.

An inspection of the water and methanol maser spectra for the 22 objects (Fig. 1), for which both types of masers are excited by the same underlying central star, reveals that in about two-thirds of the sources the water emission does not appear at the same velocities as the methanol emission. In G22.335−0.155, G23.207−0.377, G23.389+0.185, G31.581+0.077, G34.475−−0.093, G38.038−0.300, and G38.203−0.067, only a few features of both maser species coincide in velocity. Furthermore, the velocity spread of the water masers is 2–15 times larger than that of the methanol masers with the exception of G23.389+0.185, G23.707−00.198, G33.980−00.019, G36.705+0.096, G39.100++00.491. That was also found in a larger sample observed using ATCA by Breen et al. (2010). This implies that the water and methanol masers emerge from different portions of the gas surrounding the protostar. It is consistent with theoretical models proposing that radiative pumping of the CH_3OH molecule

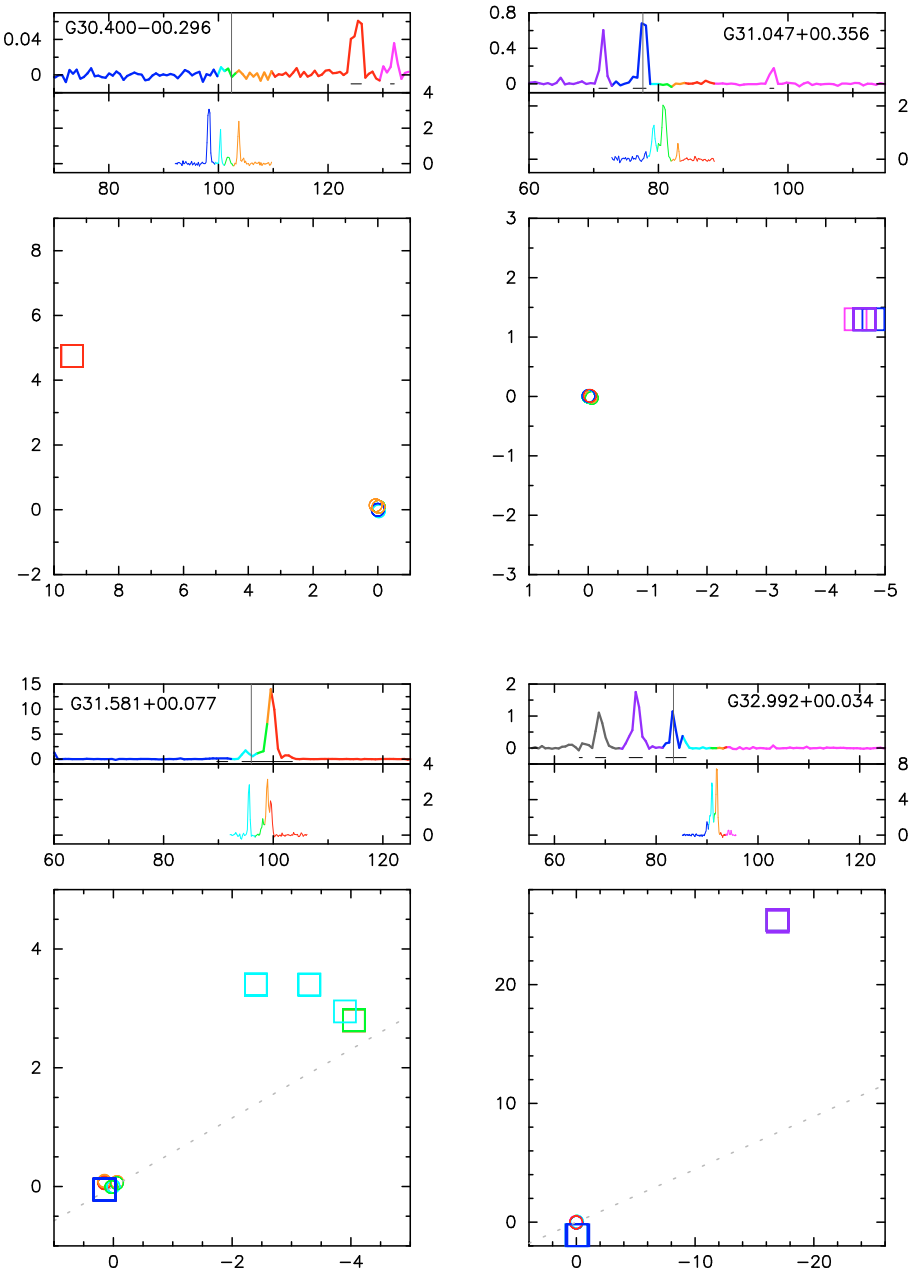

Fig. 1. continued.

occurs at temperatures lower than 150 K and densities lower than 10^8 cm^{-3} (e.g., Cragg et al. 2005, and references therein), but the collisional pumping of H_2O molecules occurs in dense (>10^8 cm^{-3}) and hot (400 K) shocked gas (Elitzur et al. 1989).

3.2. Methanol sources without water emission

Towards four sources, G23.657−0.127, G24.634−0.324, G25.411+0.105, and G27.221+0.136, no water emission was detected above a 5σ level of 15−25 mJy (Table 2). Three sources (G23.657−0.127, G24.634−0.324, and G25.411+0.105) display a ring-like structure in their 6.7 GHz methanol maser emission (Bartkiewicz et al. 2009). These morphologies have been found in at least nine out of 31 sources (Bartkiewicz et al. 2009) and was the motivation behind these follow-up observations. In addition, there are five methanol sources (G24.148−00.009, G24.541+00.312, G30.400−00.296, G31.047+00.356, and G38.038−00.300) where the water masers seem to be unassociated since the linear distance between both masers is above 0.1 pc (Table 4). Their methanol masers have linear, arched, complex/ring, ring, and complex structures, respectively (Bartkiewicz et al. 2009). For clarity, we list the morphological classification of all *methanol* masers in the last column of Table 4. We note that towards G38.038−0.300 two distinct water masers were detected with separations of about 15″, corresponding to a 0.2 pc linear separation for the near kinematic distance.

We note that emission from the 22 GHz water transition often exhibits a significant temporal variability on time scales of a few months (Brand et al. 2003). We therefore expect a number of non-detections in our sample to be different at another epoch. However, our non-detections were also not detected by a single dish study (Szymczak et al. 2005) when observed with a sensitivity of ∼1.5 Jy. Thus, the water emission in these sources may be relatively weak if present at all.

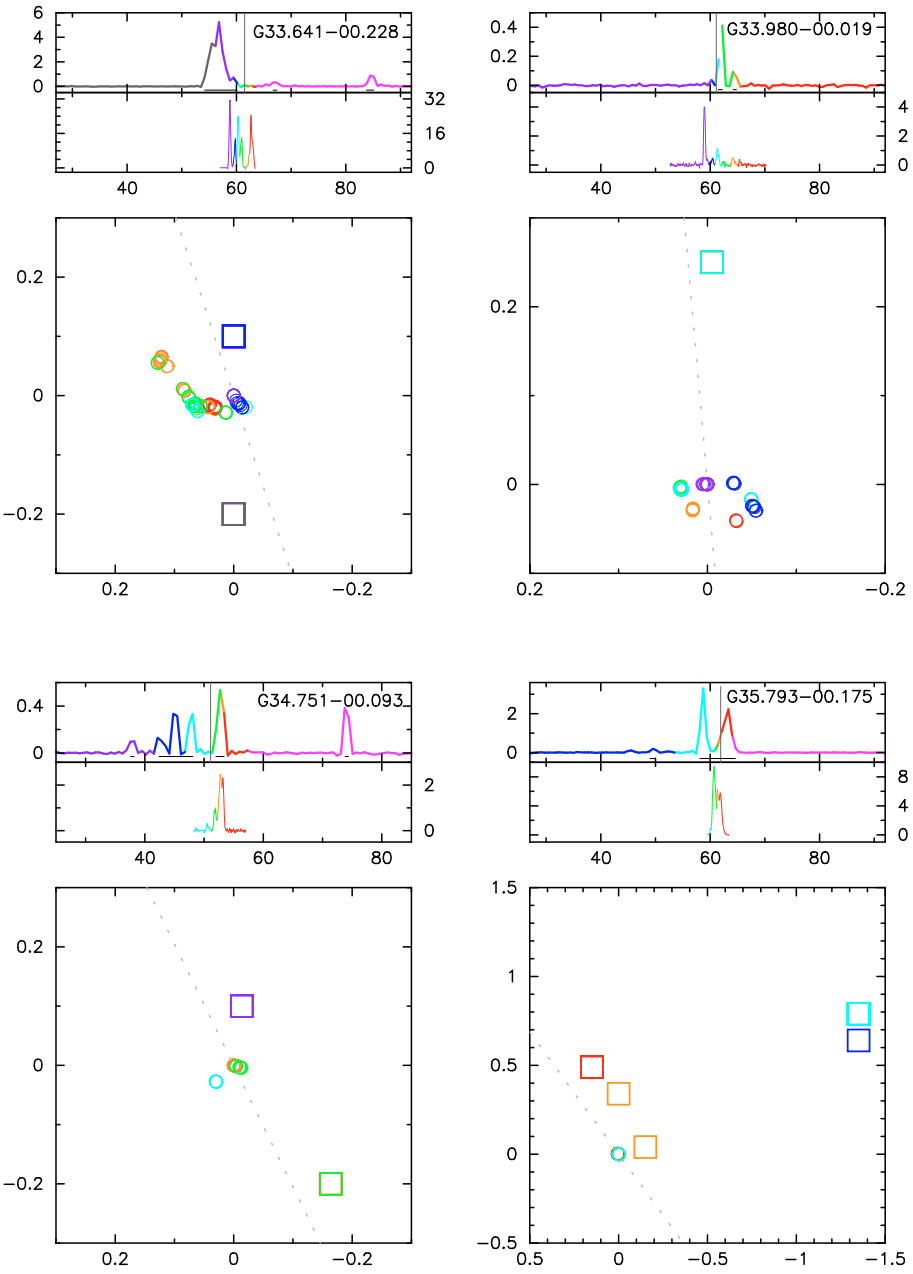

Fig. 1. continued.

3.3. Maser luminosity

We calculated the maser luminosities using the VLA data for the water maser emission and the 32 m dish observations for the methanol maser emission (Table 4). They were observed almost simultaneously (Sect. 2.2). In our sample, the *isotropic* water maser luminosity ranges from $10^{-7.4}$ to $10^{-4.6}$ $L_{\odot}$. The median luminosity of the whole sample is 10^{-6} $L_{\odot}$. We note that for all but one source G23.207−00.377, the sources with a ring morphology of methanol emission have water maser luminosities *lower* than 10^{-6} $L_{\odot}$ (Fig. 3). This suggests that these sources are associated with young massive stellar objects, in which water masers are less luminous than in the methanol sources of alternative morphology.

The water masers detected in our survey that are not associated with methanol masers have a median H_2O maser luminosity of $10^{-6.9}$ $L_{\odot}$ (Fig. 3). Thus they do not differ significantly from the luminosity of water masers associated with methanol sources. The median luminosity of methanol maser emission, estimated from single dish data, is $10^{-5.7}$ $L_{\odot}$, somewhat higher than that of the water maser emission (Fig. 3). We relate this difference to the extremely high sensitivity of the VLA observations, about 60 times higher than that reported in Szymczak et al. (2005). We do not detect any correlation between luminosities of methanol and water masers. Xu et al. (2008) found a correlation between these two measurements, although they claimed that since there were no physical connections between both lines, it might be a distance-squared effect, as suggested by Palla et al. (1991). The two maser species require different excitation conditions and, even if they are related to the same YSO (Sect. 3.1), may arise in different subregions such as discs and outflows. Xu et al. (2008) also found that water maser luminosities were higher than the methanol maser luminosities, a finding that is inconsistent with our data.

4. Discussion

4.1. Morphologies of masers and MIR counterparts

Our intention was to search for any relation between the morphology of the masers and to that of the dust. Thus, we searched

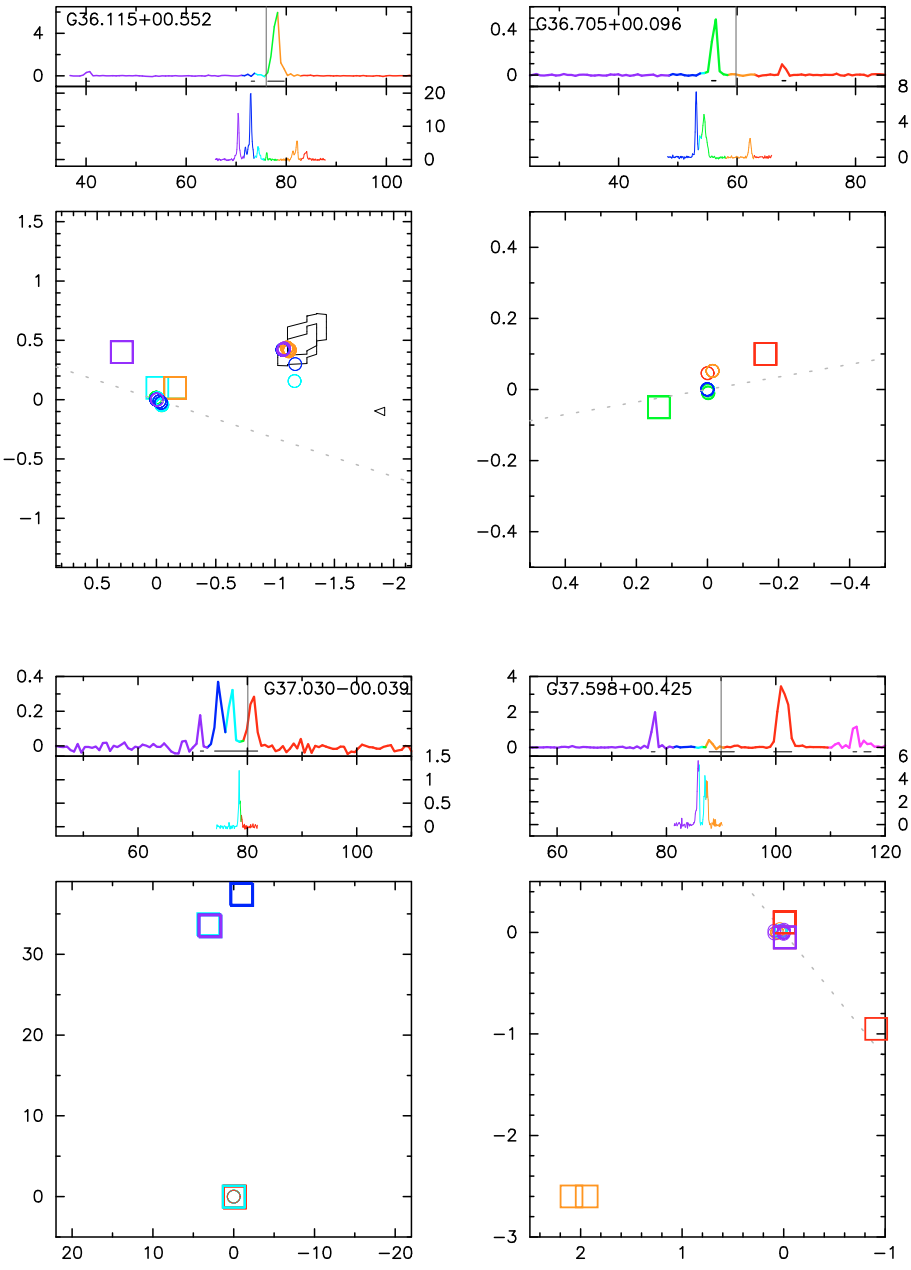

Fig. 1. continued. The radio continuum emission at the levels of 3 and 6 × $\sigma_{\rm rms}$ detected towards G36.115+00.552 is indicated by black contour lines (Bartkiewicz et al. 2009).

for mid-infrared (MIR) emission towards the detected water masers using the *Spitzer* IRAC maps[2]. We found that in total 21 out of 27 sources of water maser emission have MIR counterparts within 1.″2 arcseconds on the sky (Table 2). To clarify the nature of the studied sources, we compared the morphology of the water maser and MIR emission from maps at 4.5 μm of pixel size of 0.″6 (Fazio et al. 2004). The position angle of water maser clusters associated with the methanol source, PA_{H_2O}, was determined using a least squares fit to the maser spot distribution. For sources with a single water maser cluster, the PA_{H_2O} was assumed to be the position angle of the direction between the water maser cluster and the flux-weighted centre of the 6.7 GHz methanol maser distribution observed with the EVN (Bartkiewicz et al. 2009). The PA_{MIR} was estimated using 4.5 μm emission maps and by fitting two-dimensional Gaussian components. For several objects, these estimates are very uncertain, and we instead used the maps of the 4.5 μm–3.6 μm excess. The values of PA_{H_2O} and PA_{MIR} are listed in the last two columns of Table 2. The entries with an error of about 10−15° are given in italics. For the remaining sources, the errors in PA_{MIR} and PA_{H_2O} are smaller than 6° and 3°, respectively.

Figure 4 shows the distribution of the position angle differences. In 18 out of 21 sources, the water maser structure is aligned to within less than 20° of the extended emission at 4.5 μm. For the remaining sources the position angle differences are smaller than 47°. As the 4.5 μm emission is interpreted as a tracer of shocked H_2 in the outflow (Smith et al. 2006; Davis et al. 2007; Cyganowski et al. 2008, 2009, and references therein), our finding of the close alignment of the spatial extents of these two tracers strongly suggests that the H_2O masers originate in outflows. It is fully consistent with a theoretical model in which H_2O masers are excited by the collisional pumping of H_2 molecules in shocks associated with outflows (Elitzur et al. 1989).

The comparison of the H_2O maser morphology imaged by the VLA-CnB with that for the 6.7 GHz CH_3OH maser seen

[2] http://irsa.ipac.caltech.edu/

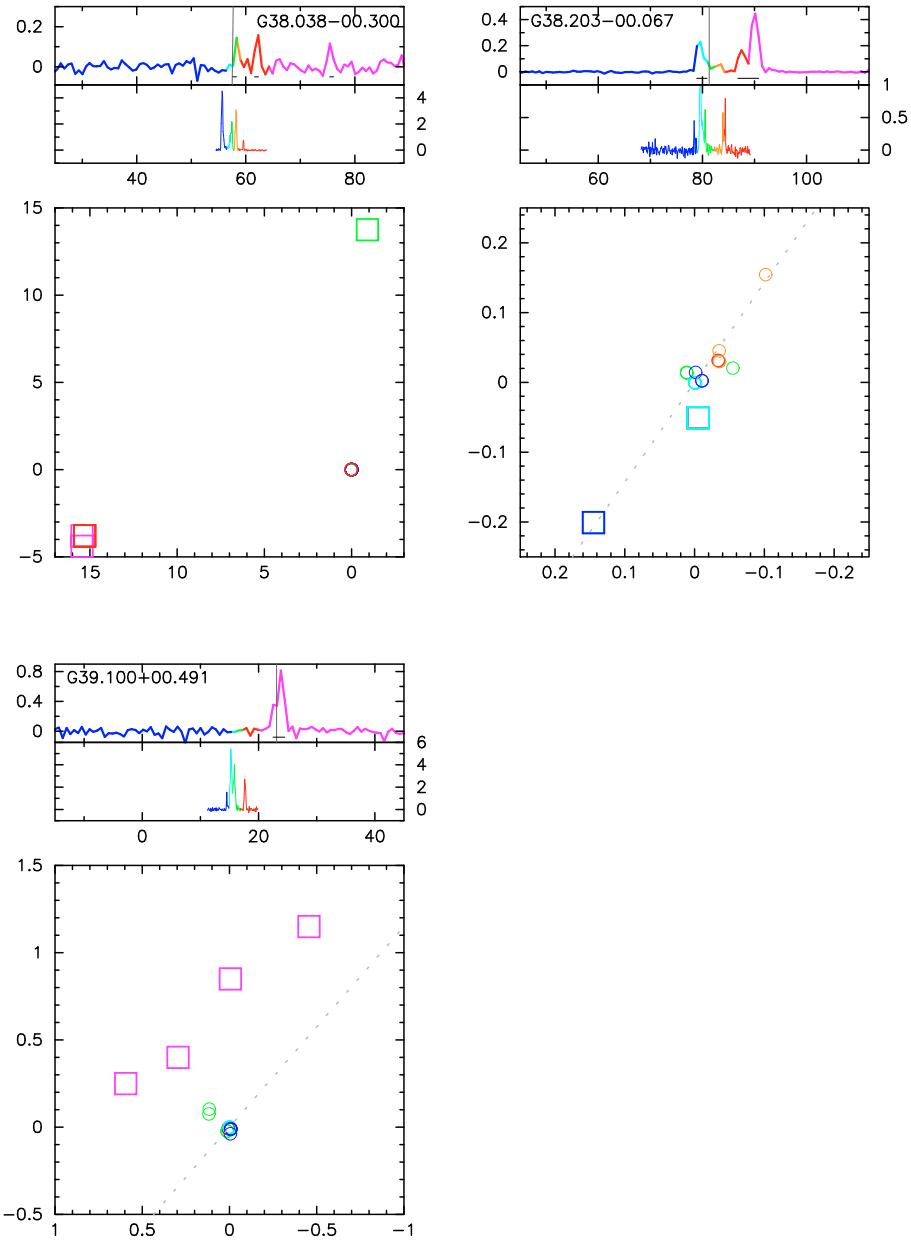

Fig. 1. continued.

with the EVN (Bartkiewicz et al. 2009) is difficult because of the larger positional uncertainty of the VLA 22 GHz data, and because a significant fraction of the 6.7 GHz flux may be missed by the milliarcsecond (mas) resolution observations. The case of G39.100+0.491 is instructive in this context; this relatively nearby source (distance 1.7 kpc) observed at 6.7 GHz with the 5×15 mas^2 EVN beam appeared as an irregular cluster of size of $0\farcs18 \times 0\farcs04$ (Bartkiewicz et al. 2009). However, using the $2\farcs4 \times 1\farcs3$ VLA beam, a much richer structure of methanol maser emission was found consisting of two bright clusters separated by $\sim 0\farcs7$ at PA of $-50°$ and diffuse emission between them (Cyganowski et al. 2009). The 6.7 GHz maser emission is clearly extended along the same position angle as the 4.5 μm emission in the *Spitzer* maps, as well as the H_2O maser emission observed here.

However, for sources with a ring-like distribution of 6.7 GHz maser emission seen at mas resolution, a comparison with the water emission structure observed with arcsecond resolution is still useful. In four out of five rings where a methanol-water maser association exists, the major axis of the methanol ring is crudely orthogonal to the main axis of the water maser structure, G23.207−0.377 is being probably the best example. These methanol masers form a ring-like structure with the PA of the major axis of $-60°$, and a velocity range of 13.20 km s^{-1}, the remainder most likely tracing an outflow (Bartkiewicz et al. 2009). The water maser emission is distributed over a region of $1\farcs5 \times 1\farcs5$ and the wider velocity range of 29 km s^{-1}. The linear size of water maser is 0.04 pc, while the methanol ring has diameter of only 0.006 pc. Since the methanol emission in a ring-like structure most likely traces a disc or torus around a massive stellar object (Bartkiewicz et al. 2009), the water maser emission along the normal to the disc appears to represent the outflow. This is supported by the morphology of detected MIR counterpart, which has a PA of 52° (Table 2). The other three sources G23.389+0.185, G33.980−0.019, and G34.751−0.093 are possible cases with a similar scenario.

We conclude that the water masers in our sample generally coincide with the MIR counterpart sources. The majority of the sources exhibit a water maser structure aligned with the extension direction of the 4.5 μm emission, while for some of

Table 3. Water maser spots detected towards the sample of 31 methanol maser sources. The absolute coordinates of the (0, 0) point for each object are listed in Table 1.

ΔRA (″)	ΔDec (″)	V_{LSR} (km s^{-1})	S (mJy beam^{-1})
G21.407−00.254			
–0.450	0.851	100.2	151.470
–0.450	0.851	99.5	290.950
–0.450	0.851	98.9	170.910
0.001	–0.049	93.6	457.630
0.001	–0.049	92.9	681.440
0.001	–0.049	92.3	319.830
G22.335−00.155			
–0.001	–0.050	35.6	169.200
–0.001	–0.050	34.9	425.210
–0.001	–0.050	32.3	112.560
–0.001	–0.050	31.0	112.750
–0.001	–0.050	29.7	402.000
–0.001	–0.050	29.0	764.310
–0.001	–0.050	28.4	55.741
G22.357+00.066			
0.007	0.101	91.5	268.630
0.007	0.101	89.6	97.639
0.157	0.251	88.9	1935.500
0.007	0.251	88.3	3136.500
0.007	0.101	87.6	1570.100
0.157	0.251	86.9	248.040
0.007	0.101	86.3	578.120
0.007	0.101	85.6	364.780
0.007	0.101	85.0	255.620
0.007	–0.049	82.3	488.520
0.007	–0.049	81.7	688.760
0.007	0.101	79.0	130.260
0.307	–0.499	76.4	170.050
0.307	–0.499	75.8	206.370
0.307	–0.499	75.1	350.030
0.307	–0.499	74.4	200.560
0.307	–0.499	73.8	179.130
0.307	–0.499	73.1	141.600
–15.309	–12.949	61.9	154.000
–15.309	–12.949	61.3	108.320
G23.207−00.377			
–0.152	–0.200	92.9	61.702
–0.152	–0.200	92.2	173.440
–0.152	–0.200	91.6	398.600
–0.152	–0.200	90.9	357.690
–0.152	–0.200	90.3	109.160
–0.152	–0.050	81.0	799.230
–0.152	–0.050	80.4	3030.800
–0.152	–0.050	79.7	6738.300
–0.152	–0.050	79.1	6281.900
–0.002	–0.050	78.4	3056.700
–0.152	–0.050	77.8	5250.100
–0.002	–0.050	77.1	6920.800
–0.152	–0.050	76.4	3010.400
–1.505	–0.950	75.8	172.700
–0.152	–0.050	75.8	217.300
–0.152	–0.050	75.1	1007.800
–1.355	–0.950	75.1	126.090
–0.152	–0.050	74.5	5069.900
–0.152	–0.050	73.8	10909.000
–0.152	–0.050	73.2	11463.000
–0.152	–0.050	72.5	5021.200
–0.152	–0.100	71.8	518.040
–0.152	–0.050	71.2	867.870
–0.152	–0.050	70.5	2283.600
–0.152	–0.050	69.9	2145.600
–0.152	–0.050	69.2	725.110

Table 3. continued.

ΔRA (″)	ΔDec (″)	V_{LSR} (km s^{-1})	S (mJy beam^{-1})
G23.207−00.377 *cont.*			
–1.505	–0.950	69.2	203.670
–0.152	–0.100	68.5	136.810
–1.204	0.400	68.5	153.120
–1.505	–0.950	68.5	79.018
–1.204	0.400	67.9	93.406
–1.204	0.400	67.2	60.951
–0.152	–0.050	66.6	62.789
–1.204	0.400	65.9	93.942
–0.152	–0.050	65.9	82.876
–1.204	0.400	65.3	238.600
–1.204	0.400	64.6	298.590
–1.204	0.400	63.9	164.130
G23.389+00.185			
0.003	–0.050	78.7	127.570
–0.147	–0.050	78.0	145.710
–0.147	–0.050	76.7	141.910
0.003	–0.050	76.1	92.012
G23.707−00.198			
0.901	0.250	74.6	155.380
0.751	0.250	73.9	97.242
3.753	–4.850	73.9	67.946
3.753	–4.850	72.6	914.740
3.753	–4.850	72.0	682.860
0.901	0.250	62.1	131.370
0.901	0.250	61.4	278.160
0.751	0.250	60.8	89.936
G23.966−00.109			
1.205	–5.450	77.2	163.090
1.055	0.250	73.9	214.070
1.055	0.250	73.3	352.120
0.005	–0.050	72.6	774.970
0.005	–0.050	72.0	385.730
0.005	–0.050	71.3	177.550
0.005	–0.050	70.7	119.670
0.005	–0.050	70.0	143.980
0.155	–0.050	69.3	111.070
1.055	0.250	54.9	221.190
1.055	0.250	54.2	193.970
1.055	0.250	53.5	106.160
1.055	0.250	52.9	129.560
1.055	0.250	51.6	104.080
0.905	0.400	50.9	122.790
1.055	0.250	48.9	1120.800
1.055	0.250	48.3	255.340
1.055	0.250	47.0	209.790
1.055	0.250	46.3	110.470
1.055	0.250	45.6	73.665
0.905	0.400	44.3	91.386
1.055	0.250	43.7	138.280
0.905	0.250	43.0	130.530
1.055	0.250	42.4	106.440
1.055	0.250	39.7	111.540
1.055	0.250	39.1	180.410
–0.295	1.150	36.4	514.030
–0.295	1.150	35.8	851.210
–0.295	1.150	35.1	407.550
–0.295	1.150	34.5	233.570
G24.148−00.009			
14.281	21.100	24.4	166.490
14.281	21.100	23.7	94.306
14.432	21.100	0.03	75.532
G24.541+00.312			
–33.616	–12.350	101.1	188.720
–33.766	–12.200	100.4	166.820

Table 3. continued.

ΔRA (″)	ΔDec (″)	V_{LSR} (km s^{-1})	S (mJy beam^{-1})
–33.766	–12.200	99.8	71.283
–33.616	–12.350	99.1	126.840
G26.598−00.024			
0.455	–0.050	22.2	1088.200
1.056	–0.200	29.5	75.790
G28.817+00.365			
–0.615	–0.449	123.6	73.343
–0.615	–0.449	123.0	74.491
–0.615	–0.049	90.7	232.440
–0.615	–0.049	90.0	606.260
–0.615	–0.049	89.4	1469.100
–0.615	–0.049	88.7	7338.900
–0.615	–0.049	88.1	13070.000
–0.615	–0.049	87.4	8506.800
–0.615	–0.049	86.8	2023.100
–0.465	–0.499	86.1	893.090
–1.665	–0.199	86.1	354.630
–0.315	–0.349	85.4	1251.800
–1.665	–0.199	85.4	285.680
–0.465	–0.499	84.8	1088.800
–0.465	–0.499	84.1	955.240
–0.465	–0.499	83.5	763.940
–1.665	–0.199	83.5	387.630
–0.615	–0.199	82.8	335.700
–1.665	–0.199	82.8	407.980
–1.665	–0.199	82.1	328.380
–1.665	–0.199	82.8	407.980
–0.615	–0.199	82.8	335.700
–1.665	–0.199	82.1	328.380
–0.765	–0.499	81.5	282.630
–1.665	–0.199	81.5	231.990
–0.765	–0.499	80.8	641.910
–1.665	–0.199	80.8	196.730
–0.765	–0.499	80.2	630.590
–1.665	–0.199	80.2	446.670
–1.815	–0.349	79.5	806.980
–0.615	–0.199	79.5	280.910
–1.815	–0.349	78.9	914.610
–1.815	–0.349	78.2	691.990
–1.815	–0.349	77.5	454.190
–1.815	–0.349	76.9	430.300
–1.815	–0.349	76.2	375.960
–0.615	–0.199	76.2	228.730
–0.615	–0.199	75.6	261.780
–0.615	–0.199	74.9	202.850
–0.765	–0.349	69.0	140.150
–0.765	–0.349	68.3	218.480
–0.765	–0.349	67.7	180.120
–0.765	–0.349	59.1	209.740
–0.765	–0.349	58.4	510.720
–0.765	–0.349	57.8	558.730
–0.765	–0.349	57.1	282.790
G30.318+00.070			
–0.903	0.400	52.6	474.730
–0.903	0.400	51.9	291.770
–0.903	0.400	51.2	384.570
–0.903	0.400	50.6	235.530
–0.903	0.400	49.9	2807.700
–0.903	0.400	49.3	2283.700
–0.903	0.400	47.9	2274.500
–0.903	0.400	47.3	2013.200
–0.903	0.400	46.6	224.420
–0.903	0.400	46.0	878.560
–0.903	0.400	45.3	925.040
–0.003	–0.200	32.8	511.840

Table 3. continued.

ΔRA (″)	ΔDec (″)	V_{LSR} (km s^{-1})	S (mJy beam^{-1})
–0.003	–0.200	32.2	554.200
G30.400−00.296			
9.441	4.751	132.1	46.758
9.441	4.751	126.1	68.852
9.441	4.751	125.5	77.645
9.441	4.751	124.8	53.516
9.441	4.751	124.2	52.276
G31.047+00.356			
–4.502	1.300	97.8	173.050
–4.802	1.300	78.1	629.490
–4.802	1.300	77.4	669.660
–4.652	1.300	76.8	66.542
–4.652	1.300	76.1	91.005
–4.652	1.300	72.1	79.039
–4.652	1.300	71.5	558.540
–4.652	1.300	70.8	140.980
G31.581+00.077			
0.149	–0.050	103.5	239.060
0.149	–0.050	102.8	621.510
0.149	–0.050	102.2	711.120
0.149	–0.050	101.5	350.840
–4.051	2.800	100.9	1698.600
–4.051	2.800	100.2	9004.900
–4.051	2.800	99.5	12545.000
–4.051	2.800	98.9	6135.200
–4.051	2.800	98.2	1318.600
–4.051	2.800	97.6	827.400
–3.301	3.400	96.9	536.440
–3.901	2.950	96.9	486.450
–3.301	3.400	96.3	275.000
–2.401	3.400	95.6	951.870
–2.401	3.400	94.9	1602.100
–2.401	3.400	94.3	789.870
0.149	–0.050	91.7	135.530
0.149	–0.050	91.0	136.240
0.149	–0.050	90.3	124.820
0.149	–0.050	89.7	121.650
G32.992+00.034			
–0.013	–1.100	85.9	172.460
–0.013	–1.100	85.2	366.940
–0.163	–1.100	83.9	162.740
–16.963	25.450	83.9	500.950
–16.963	25.450	83.2	1070.200
–16.963	25.450	82.6	164.750
–16.963	25.450	81.9	135.560
–16.963	25.450	77.3	337.560
–16.963	25.450	76.7	1214.400
–16.963	25.450	76.0	1606.000
–16.963	25.450	75.3	532.860
–16.963	25.300	74.7	329.590
–16.963	25.450	70.1	324.050
–16.963	25.450	69.4	621.300
–16.963	25.450	68.8	1049.600
–16.963	25.450	68.1	537.610
–16.963	25.450	65.5	146.450
G33.641−00.228			
0.000	0.100	85.1	767.180
0.000	0.100	84.5	892.410
0.000	0.100	83.8	211.630
0.000	0.100	67.4	316.000
0.000	0.100	66.7	318.810
0.000	0.100	60.1	274.990
0.000	0.100	59.5	705.260

Table 3. continued.

ΔRA (″)	ΔDec (″)	V_{LSR} (km s^{-1})	S (mJy beam^{-1})
0.000	–0.200	58.8	471.010
0.000	–0.200	58.1	1393.500
0.000	–0.200	57.5	2696.100
0.000	–0.200	56.8	5117.600
0.000	–0.200	56.2	3317.100
0.000	–0.200	55.5	3500.900
0.000	–0.200	54.9	21800.300
0.000	–0.200	54.2	745.680
G33.980−00.019			
–0.005	0.250	64.8	56.244
–0.005	0.250	64.2	90.924
–0.005	0.250	62.2	398.350
–0.005	0.250	61.5	181.850
G34.751−00.093			
–0.014	0.100	74.4	293.360
–0.014	0.100	73.8	379.520
–0.164	–0.200	53.4	344.340
–0.164	–0.200	52.7	525.630
–0.164	–0.200	52.0	200.420
–0.014	0.100	48.1	333.880
–0.014	0.100	47.4	249.800
–0.014	0.100	45.5	306.860
–0.014	0.100	44.8	331.100
–0.014	0.100	42.8	102.260
–0.014	0.100	42.2	123.410
–0.014	0.100	38.2	89.800
–0.014	0.100	37.6	97.497
G35.793−00.175			
0.150	0.490	64.6	170.640
0.150	0.490	64.0	641.760
0.150	0.490	63.3	1645.500
0.150	0.490	62.7	1090.200
–0.150	0.040	62.0	637.780
0.000	0.340	61.4	205.560
–1.350	.790	60.7	67.977
–1.350	.790	59.4	571.250
–1.350	.790	58.7	2388.400
–1.350	.790	58.1	729.820
–1.350	.640	49.5	181.000
G36.115+00.552			
–0.157	0.100	79.6	606.160
–0.157	0.100	78.9	1175.100
–0.157	0.100	78.3	4908.200
–0.157	0.100	77.6	38430.600
–0.157	0.100	76.9	1576.100
–0.157	0.100	76.3	260.940
–0.007	0.100	73.7	185.700
0.293	0.400	40.7	351.430
0.293	0.400	40.1	379.110
G36.705+00.096			
–0.163	0.100	68.2	54.737
–0.163	0.100	67.6	106.380
0.137	–0.050	56.4	548.860
0.137	–0.050	55.7	332.540
G37.030−00.039			
–0.155	–0.150	81.9	74.981
–0.005	0.000	81.2	266.990
–0.155	0.000	80.6	194.320
–0.155	0.000	79.9	87.324
–0.005	0.000	77.3	122.670
2.847	33.450	77.3	122.910
–0.005	0.000	76.6	212.280
3.147	33.750	76.6	111.340
2.997	33.600	76.0	102.090
2.997	33.600	75.3	85.365
–0.906	37.500	75.3	79.832

Table 3. continued.

ΔRA (″)	ΔDec (″)	V_{LSR} (km s^{-1})	S (mJy beam^{-1})
–1.056	37.350	74.7	260.000
–1.056	37.350	74.0	96.094
2.847	33.450	72.0	46.063
2.997	33.600	71.4	88.134
G37.598+00.425			
–0.011	0.100	117.4	219.240
–0.011	0.100	116.7	242.660
–0.011	0.100	116.1	318.110
–0.011	0.100	114.8	1031.300
–0.011	0.100	114.1	1030.300
–0.011	0.100	102.9	498.890
–0.011	0.100	102.3	2173.000
–0.011	0.100	101.6	2605.600
–0.011	0.100	100.9	2909.000
–0.011	0.100	100.3	1711.500
–0.011	–0.050	99.6	295.040
–0.911	–0.950	92.4	106.880
1.940	–2.600	88.4	173.860
2.090	–2.600	87.8	372.810
–0.011	–0.050	77.9	1780.700
–0.011	–0.050	77.2	761.960
G38.038−00.300			
15.451	–3.801	76.1	69.425
15.451	–4.401	75.4	108.680
15.301	–3.801	62.3	149.360
15.301	–3.801	61.6	79.108
–0.908	13.749	58.3	141.580
G38.203−00.067			
–0.005	–0.051	90.8	390.370
–0.005	–0.051	90.1	628.690
0.145	–0.201	89.5	510.060
–0.005	–0.051	88.2	158.110
–0.005	–0.051	87.5	235.350
–0.005	–0.051	86.8	154.100
–0.005	–0.051	80.9	120.230
–0.005	–0.051	80.3	161.100
0.145	–0.201	79.6	331.320
0.145	–0.201	78.9	275.340
G39.100+00.491			
0.295	0.400	24.5	255.050
0.595	0.250	23.9	637.950
–0.005	0.850	23.2	223.880
–0.456	1.150	22.5	289.050

the objects in which the methanol masers trace circumstellar discs/tori, the water masers appear to be aligned in the orthogonal direction. In general, this is consistent with previous observations indicating that MIR emission is indeed associated with water masers, and their relative distributions imply that water masers originate in outflows (e.g., De Buizer et al. 2005).

Assuming that the methanol emission arises close to the protostar, while H_2O masers trace outflows further away from the central object, the size of the outflows can be estimated for 22 sources where a methanol-water maser association exists. Our data imply size scales for the outflows from 0.0006 pc to 0.13 pc with a median and mean values of 0.01 ps and 0.022 pc, respectively. We note that three sources G22.335−0.155, G30.400−0.296, and G33.980−00.019 are unresolved with a 1.″4×0.″8 beam. Their velocities range from 3.3 km s^{-1} to 7.9 km s^{-1} (Table 3), which may also be indicative of outflows along the line of sight. However, we need to verify this hypothesis using VLBI observations.

Table 4. Characteristic parameters of the sources observed.

Source Gll.lll±bb.bbb	V_{sys} (km s^{-1})	D_{near} (kpc)	$\Delta_{wm_{dist}}$ (pc)	$\log(L_{H_2O})^{a,b}$ ($L_\odot$)	$\log(L_{H_2O})^{c}$ ($L_\odot$)	$\log(L_{CH_3OH})$ ($L_\odot$)	Class[1]
G21.407−00.254	90.7	5.12	0.00074	−6.02		−5.34	C
G22.335−00.155	30.9	2.47	0.00012	−6.79		−6.04	L
G22.357+00.066	84.2	4.86	0.00094	−5.37	−7.03	−5.58	C
G23.207−00.377	78.9	4.63	0.00135	−4.56		−5.05	R
G23.389+00.185	74.8	4.47	0.00065	−6.89		−5.14	R
G23.657−00.127	82.4	3.19[2]		−8.15↓		−5.60	R
G23.707−00.198	68.9	4.22	0.01575	−6.63	−6.34	−5.13	A
G23.966−00.109	72.7	4.37	0.00063	−5.57		−5.74	L
G24.148−00.009	23.1	1.92	0.23736	−8.22↓	−7.77	−7.23	L
G24.541+00.312	107.8	5.70	0.98931	−8.30↓	−6.92	−5.17	A
G24.634−00.324	42.7	3.00		−8.22↓		−6.48	R
G25.411+00.105	96.0	5.25		−7.70↓		−5.70	R
G26.598−00.024	23.3	1.85	0.00126	−7.42		−6.54	R
G27.221+00.136	112.6	6.04		−7.40↓		−5.21	C
G28.817+00.365	87.0	4.90	0.00879	−4.72		−6.34	A/R
G30.318+00.070	45.3	2.97	0.00288	−5.74		−6.77	L
G30.400−00.296	102.4	5.76	0.29322	−8.30↓	−6.89	−5.80	C/R
G31.047+00.356	77.6	4.51	0.10145	−6.05		−6.16	R
G31.581+00.077	96.0	5.49	0.00293	−4.70		−5.82	A/R
G32.992+00.034	83.4	4.88	0.02508	−6.53	−5.44	−5.75	C
G33.641−00.228	61.5	3.77	0.00183	−5.30		−4.88	A
G33.980−00.019	61.1	3.75	0.00455	−6.80		−6.35	R
G34.751−00.093	51.1	3.24	0.00157	−6.22		−6.35	R
G35.793−00.175	61.9	3.83	0.00297	−5.56		−5.53	L
G36.115+00.552	76.0	4.66	0.00203	−5.29		−5.29	P
G36.705+00.096	59.8	3.75	0.00273	−6.64		−6.40	C
G37.030−00.039	80.1	5.02	0.00024	−6.34	−6.30	−5.47	S
G37.598+00.425	90.0	6.36	0.00154	−4.96	−6.51	−5.26	C
G38.038−00.300	57.5	3.66	0.24487	−8.00↓	−7.47; −7.10	−5.96	C
G38.203−00.067	81.3	5.31	0.00129	−6.00		−5.66	C
G39.100+00.491	23.1	1.70	0.00288	−7.06		−6.29	C

Notes. [1] Class of morphology of *methanol* masers: S – simple, L – linear, R – ring, C – complex, A – arched, P -pair (Bartkiewicz et al. 2009). [2] Distance based on the trigonometric parallax (Bartkiewicz et al. 2008). [(a)] Luminosity of water maser associated with the methanol source. In a few cases (e.g., G22.357+00.066) only some spots lie in the close surroundings of methanol emission (Fig. 1). [(b)] The upper limit is marked by symbol ↓. It means we did not register the water maser spots coinciding with methanol masers. [(c)] Luminosity of water maser unassociated or likely to be unassociated with a methanol source.

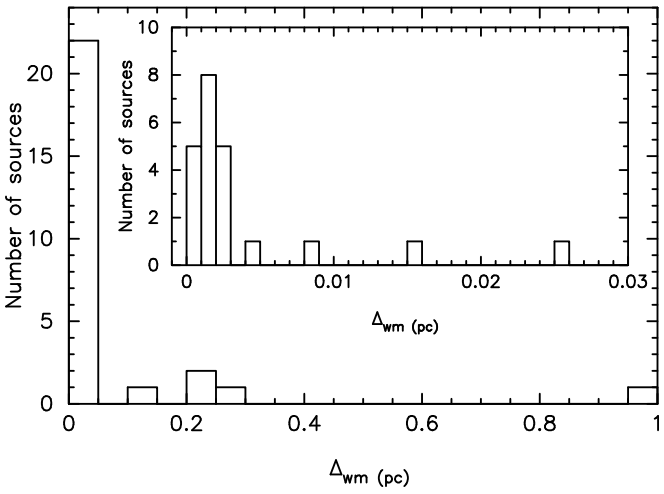

Fig. 2. Histogram of linear separations between the water and methanol masers for the sample. The inset is the enlargement of the histogram for the first bin.

4.2. Signposts of multiple active centres

Water maser emission was detected towards 12 of the methanol targets in distinct clusters separated from methanol maser spots by >0.1 pc. In two objects G37.030−00.039 and G38.038−00.300, we observed two water clusters that are significantly separated from each other. We therefore found in total that 14 water maser clusters in our sample are located at significant distances from methanol maser spots (Table 5). This characteristic was also noticed in studies by Breen et al. (2010) using ATCA.

For these objects, we also inspected *Spitzer* IRAC maps to search for MIR counterparts to the water maser clusters. The results are summarized in Table 5. We found that 10 of the 14 clusters have MIR counterparts that, within the measurement uncertainties, do not coincide with the methanol maser clusters and their MIR counterparts reported in Bartkiewicz et al. (2009). We therefore conclude that in these 10 cases both types of masers, methanol and water, are not associated with the same MIR object. It is possible that both masers are associated with the same molecular cloud where star formation takes place, but do not trace the environment of the same protostar. They very likely trace different protostars as most of them have MIR properties typical of embedded young massive objects and display a 4.5 μm−3.6 μm excess that is an indicator of shocked material in outflows (e.g., Cyganowski et al. 2008). The remaining four water maser clusters lying 0.1–0.3 pc from the methanol maser spots (G23.966−00.109, G31.581+00.077, G37.598+00.425, and tentatively G31.047+00.356) (Table 5)

Table 5. List of methanol maser sources with the water maser emission of linear offset greater than 0.1 pc.

CH_3OH source Gll.lll±bb.bbb	H_2O emission Gll.lll±bb.bbb	$\Delta_{wm_{dist}}$ (arcsec)	(pc)	ΔV_{min} (km s^{-1})	ΔV_{max} (km s^{-1})	MIR source	Δ(MIR−H_2O) (arcsec)
G22.357+00.066	G22.351+0.068	20.05	0.47	22.3	22.9	G022.3506+00.0678	3.2[2]
G23.707−00.198	G23.706−0.200	6.13	0.13	3.1	5.0	G023.7057-00.1999	1.3[2]
G23.966−00.109	G23.965−0.110	5.58	0.12	4.5*		G023.9649-00.1104	0.6[2]
G24.148−00.009	G24.155−0.010	25.48	0.24	0.6	23.1	G024.1550-00.0119	7.3[4]
G24.541+00.312	G24.534+0.319	35.90	0.99	6.7	8.7	G024.5351+00.3190	5.1[3]
G30.400−00.296	G30.403−0.297	10.57	0.29	21.8	29.7	G030.4010-00.2960	7.9[2]
G31.047+00.356	G31.047+0.357	6.91	0.11	0.2	20.2	G031.0467+00.3574	[5]
G31.581+00.077	G31.581+0.078	4.92	0.13	1.7	4.9	G031.5813+00.0788	2.3[1]
G32.992+00.034	G32.996+0.041	30.58	0.72	0.2	17.9	G032.9962+00.0414	0.3[2]
G37.030−00.039	G37.039−0.035	33.73	0.82	2.8	8.7	G037.0385-00.0350	1.6[2]
	G37.039−0.034	37.36	0.91	4.8	6.1	G037.0385-00.0350	6.1[2]
G37.598+00.425	G37.597+0.424	3.34	0.10	1.6	2.2	G037.5978+00.4253	4.1[1]
G38.038−00.300	G38.038−0.305	16.06	0.28	4.1	18.6	G038.0384-00.3042	1.6[2]
	G38.041−0.298	13.78	0.24	0.8*		G038.0409-00.2968	5.2[2]

Notes. The two first columns list the galactic coordinates of methanol and water masers, respectively. $\Delta_{wm_{dist}}$ is the angular (Col. 3) and linear (Col. 4) separation of H_2O maser emission from the methanol source. ΔV_{min} is the minimum and ΔV_{max} is the maximum differences between the LSR velocity of water maser spot from the analysed group and the systemic velocity (Table 4). The name of MIR source nearby to the H_2O maser emission and angular separation between them, Δ(MIR−H_2O), are given. [1] H_2O maser emission is associated with the same MIR source as CH_3OH maser emission. [2] H_2O maser emission is not associated with the same MIR source as CH_3OH maser emission. [3] H_2O maser emission is not associated with the same MIR source as CH_3OH maser emission, but lies instead in a cluster of three MIR sources. [4] H_2O maser emission is likely not associated with the same MIR source as CH_3OH maser emission but with MIR object in the region of diffuse (∼10″) excess of 4.5 μm emission seen in the IRAC Spitzer maps. The name of the strongest MIR counterpart is given. [5] H_2O maser emission is tentatively associated with the same MIR source as CH_3OH maser emission, lying at the edge of diffuse excess of 4.5 μm emission from possible cluster of MIR sources. * When a single maser spot was observed, only ΔV_{min} is given.

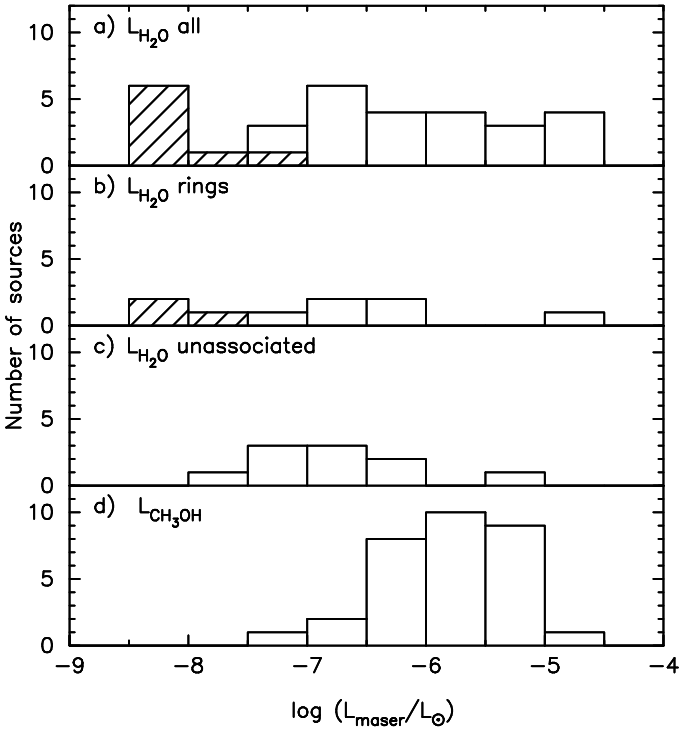

Fig. 3. **a)** Histogram of the water maser luminosity in the 6.7 GHz methanol maser sample (Table 4. The dashed bars mark sources with the upper luminosity limits (non detections). **b)** Same as in **a)** but for the sources with ring-like distribution of methanol emission. **c)** Same as in **a)** but for the water maser sources not associated with the methanol masers. **d)** Histograms of methanol maser luminosity in the sample.

are likely associated with the same MIR objects as the methanol emission.

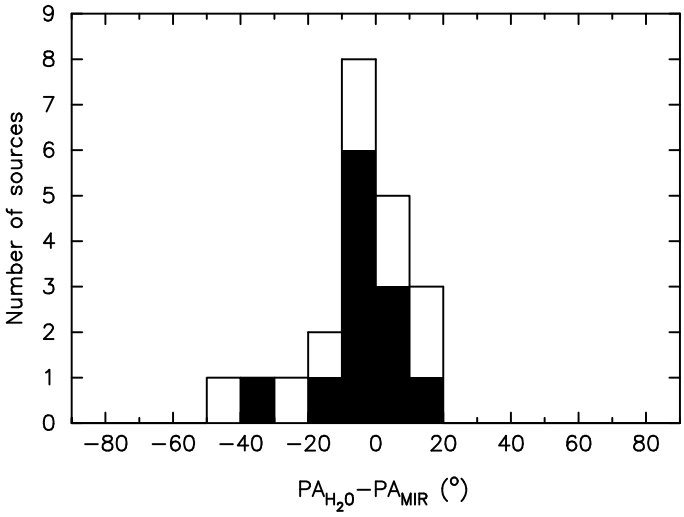

Fig. 4. Histogram of the differences in the position angles of major axes of water maser distribution and 4.5 μm emission excess for the studied objects. The sources with small errors in PA_{MIR} are indicated by the solid histogram.

4.3. Association and non-association with H II regions

In our previous VLA project, we searched for the 8.4 GHz continuum emission towards the methanol masers considered here with the sensitivity level of 0.15 mJy beam^{-1} (Bartkiewicz et al. 2009). In total, we detected eight sources towards the sample. Only in four cases was the continuum emission associated with the methanol sources. In the present study, we note that in three of these four objects the methanol structures are also associated with the distribution of water masers (Fig. 1). Therefore, both types of maser are likely to be physically connected with the radio continuum emission. One example is G28.817+0.365

where methanol spots are distributed along a PA of +45°. They are projected onto the central part of a H II region. Water masers are distributed along a PA of −89° and are spread in the SW direction from the radio continuum source. This a distribution of masers may be consistent with an outflow scenario for both masers. But proper motion studies are needed to verify that a scenario similar to that for example presented for 12 GHz methanol masers in Moscadelli et al. (2002). We note that the MIR counterpart is aligned with a PA of −88° (Table 2) and its properties are consistent with the outflow hypothesis.
Two other sources with detected H II regions, G26.598−00.024 and G36.115+00.552, have similar characteristics. Here, the overall distributions of methanol and water masers are crudely aligned in the same direction as the MIR counterparts (Table 2). In these cases, masers are displaced from the centres of the radio continuum sources by 0.007 and 0.02 pc, respectively. We suggest that these three objects support the hypothesis that we observed HMSFRs at different evolutionary stages in our sample. Beuther & Shepherd (2005) presented a scenario for the evolution of massive outflows. When a B star forms via accretion from a disc and the H II region has not yet formed, the disc-outflow interaction produces a collimated outflow. With time, a hypercompact H II region forms and the wind from the massive young star produces a less collimated outflow. The disc begins to be destroyed and an outflow with a small degree of collimation dominates the system. In sources with methanol maser rings, we detected water maser emission either not at all or relatively weakly. In sources with H II counterparts, the methanol maser morphology is less regular (although G26.598−00.024 was classified as a ring, we note that it consists of only three cluster of masers), and water-methanol maser spot distributions may also be consistent with an outflow scenario (Fig. 1).

In eight out of nine objects for which no water was found (Sect. 3.2), no continuum emission at 8.4 GHz above ∼0.15 mJy beam^{-1} was detected. The one exception is G24.148−00.009, which has weak and compact emission ($S_{\rm p}$ = 1.05 mJy beam^{-1}; $S_{\rm int}$ = 1 mJy; Bartkiewicz et al. 2009). We also note that towards that source we did not detect any water maser within 0.24 pc. This result conflicts with that of Beuther et al. (2002), who found that methanol masers are associated with cm emission only if there are nearby water masers. However, as noted by these authors, in the archetypical star-forming region W3(OH) a situation similar to that of G24.148−00.009 exists, where the methanol masers are associated with an ultracompact H II region and the water masers are offset significantly from the methanol masers and associated with a different young star (Menten 1996).

The absence of continuum emission and water masers may lend support to the hypothesis that 6.7 GHz methanol masers trace an earlier evolutionary phase than water masers where no outflows have yet started (e.g., Ellingsen et al. 2007). For the (≈50% of) methanol masers not associated with H II regions (and water emission) that show ring-like structures, we suggest that they trace circumstellar discs/tori, probably at an early stage of evolution. A less regular methanol morphology would appear at later stages and be related to outflows traced by water masers. Comparative studies of water and methanol masers in the giant molecular cloud G333.6−0.2 have suggested a similar conclusion that 6.7 GHz methanol masers trace an earlier evolutionary phase of high-mass star formation than luminous water masers do (Breen et al. 2007; Ellingsen et al. 2007). It is interesting that in four of five ring-like methanol sources, the associated water masers are weaker than the methanol masers. This supports the above-mentioned scenario that an early evolutionary stage is represented by these sources, as they may be examples of outflows just beginning. Only one ring-like source (G23.207−0.377) does not follow this trend, since its methanol emission is much weaker than the water emission. However, we note that in the distribution of methanol maser spots in this source one can see components that may belong to the outflow part traced also by water emission (Fig. 1). Therefore, this object is probably more evolved that the rest sources with ring-like morphology of the methanol emission. We discuss this source in more details in Sect. 4.1.

The aforementioned interpretation of evolutionary stage relies basically on the lack of detectable continuum at centimetre wavelengths. This may be misleading since only the most compact continuum emission was mapped. For G22.357+0.066, observations using the VLA at 8.4 GHz with a synthesized beam of 2.″3 and a sensitivity of 0.3 mJy beam^{-1}, identified a complex and extended source with a peak flux of 1.02 mJy beam^{-1}, which represents a 3σ detection (van der Walt et al. 2003). However, no emission was found at the same frequency with a beam of 0.″35 × 0.″25 and a sensitivity of 0.15 mJy beam^{-1} (Bartkiewicz et al. 2009). The methanol emission is offset by ∼15″ from the radio continuum peak, corresponding to a projected linear distance of 0.35 pc. We therefore suggest that additional sensitive searches for millimeter and centimetre continuum counterparts of ring-like methanol sources will be important to understand their nature.

5. Conclusions

High sensitivity VLA observations of the 22 GHz water maser line towards 31 methanol maser objects have yielded 27 detections, out of which 15 have been detected for the first time. Most (71%) of the methanol sources have corresponding water masers at a projected separation of less than 0.026 pc. These sources are either excited by the same underlying central object or come from different, but closely projected YSOs. We have identified MIR counterparts of 21 water masers from *Spitzer* IRAC maps. The water maser structures are well aligned with the extended emission at 4.5 μm for a large fraction (18/21) of the studied objects. This confirms that the water masers originate in outflows.

A distinct group of sources with a ring-like methanol maser distribution, likely tracing a circumstellar disc/torus around high-mass young stellar objects, have either no associated water masers at all (4 out 9), or a water maser distribution that is orthogonal to the major axis of the methanol ring (4 out 9). Moreover, the majority of this group of objects (8 out 9) does not show detectable continuum emission at 8.4 GHz and may represent an early phase of evolution. One methanol ring, G26.598−00.024, lies at the edge of a H II region and is aligned with associated water masers. Both masers water and methanol masers probably form in outflows.

We conclude that massive star-forming regions that contain methanol masers with ring-like morphologies are at the earliest evolutionary states when the young star is still forming, possibly via accretion from a disc. When winds begin to dominate, the regular ring-like structure is destroyed and methanol and water masers appear to be associated with the outflow. Additional deep observations of these sources in the radio continuum as well as in the infrared range are required to explain their nature.

Acknowledgements. A.B. and M.S. acknowledge support by the Polish Ministry of Science and Higher Education through grant N N203 386937. A.B. acknowledges support by the Nicolaus Copernicus University grant 364-A (2009).
The Very Large Array (VLA) of the National Radio Astronomy Observatory is a facility of the National Science Foundation operated under cooperative

agreement by Associated Universities, Inc. This research has made use of the NASA/IPAC Infrared Science Archive, which is operated by the Jet Propulsion Laboratory, California Institute of Technology, under contract with the National Aeronautics and Space Administration.

References

Bartkiewicz, Brunthaler, A., Szymczak, M., van Langevelde, H. J., & Reid, M. J. 2008, A&A, 490, 787
Bartkiewicz, A., Szymczak, M., van Langevelde, H. J., Richards, A. M. S., & Pihlström, Y. M. 2009, A&A, 502, 155
Beuther, H., & Shepherd, D. 2005, in Cores to Clusters: Star Formation with Next Generation Telescopes, ed. M. S. Nanda Kumar et al., Reprinted from Astrophysics and Space Sience Library (New York: Springer), 324
Beuther, H., Walsh, A., Schilke, P., et al. 2002, A&A, 390, 289
Brand, J., Cesaroni, R., Comoretto, G., et al. 2003, A&A, 407, 573
Breen, S. L., Ellingsen, S. P., Johnston-Hollitt, M., et al. 2007, MNRAS, 377, 491
Breen, S. L., Caswell, J. L., Ellingsen, S. P., & Phillips, C. J. 2010, MNRAS, 406, 1487
Caswell, J. L., Vaile, R. A., Ellingsen, S. P., Whiteoak, J. B., & Norris, R. P. 1995, MNRAS, 272, 96
Cragg, D. M., Sobolev, A. M., & Godfrey, P. D. 2005, MNRAS, 360, 533
Cyganowski, C. J., Whitney, B. A., Holden, E., et al. 2008, AJ, 136, 2391
Cyganowski, C. J., Brogan, C. L., Hunter, T. R., & Churchwell, E. 2009, ApJ, 702, 1615
De Buizer, J. M., & Minier, V. 2005, ApJ, 628, L151
De Buizer, J. M., Radomski, J. T., Telesco, C. M., & Piña, R. K. 2005, ApJSS, 156, 179
Davis, C. J., Kumar, M. S. N., Sandell, G., et al. 2007, MNRAS, 374, 29
Dodson, R., Ojha, R., & Ellingsen, S. P. 2004, MNRAS, 351, 779
Ellingsen, S. P., Voronkov, M. A., Cragg, D. M., et al. 2007, Astrophysical Masers and their Environments, ed. J. M. Chapman, & W. A. Baan (Cambridge: Cambridge Univ. Press), IAU Symp., 242, 213
Elitzur, M., Hollenbach, D. J., & McKee, C. F. 1989, ApJ, 346, 983
Fazio, G. G., Hora, J. L., Allen, L. E., et al. 2004, ApJS, 154, 10
McCaughrean, M., & Stauffer, J. 1994, AJ, 108, 1382
Menten, K. M. 1991, ApJ, 380, L75
Menten, K. 1996, in IAU Symp 178., ed. Ẽ. van Dishoek, 163
Minier, V., Booth, R. S., & Conway, J. E. 2000, A&A, 362, 1093
Moscadelli, L., Menten, K. M., Walmsley, C. M., & Reid, M. J. 2002, ApJ, 564, 813
Moscadelli, L., Goddi, C., Cesaroni, R., Beltrán, M. T., & Furuya, R. S. 2007, A&A, 472, 867
Norris, R. P., Byleveld, S. E., Diamond, P. J., et al. 1998, ApJ, 508, 275
Pestalozzi, M. R., Elitzur, M., Conway, J. E., & Booth, R. S. 2004, ApJ, 603, L113
Palla, F., Brand, J., Cesaroni, R., et al. 1991, A&A, 246, 249
Philips, C. J., Norris, R. P., Ellingsen, S.P, & McCulloch, P. M. 1998, MNRAS, 300, 1131
Pillai, T., Wyrowski, F., Menten, K. M., & Krügel, E. 2006, A&A, 447, 929
Reid, M. J., Menten, K. M., Zheng, X. W., et al. 2009, ApJ, 700, 137
Rygl, K. L. J., Brunthaler, A., Reid, M. J., et al. 2010, A&A, 511, A2
Smith, H. A., Hora, J. L., Marengo, M., & Pipher, J. L. 2006, ApJ, 645, 1264
Stahler, S., Palla, F., & Ho, P. 2000, in Protostars & Planets IV (The University of Arizona Press)
Sridharan, T. K., Beuther, H., Schilke, P., Menten, K. M., & Wyrowski, F. 2002, ApJ, 566, 931
Szymczak, M., Kus, A. J., Hrynek, G., Kepa, A., & Pazderski, E. 2002, A&A, 392, 277
Szymczak, M., Pillai, T., & Menten, K. M. 2005, A&A, 434, 613
Szymczak, M., Bartkiewicz, A., & Richards, A. M. S. 2007, A&A, 468, 617
Urquhart, J. S., Hoare, M. G., Lumsden, S. L., et al. 2009, A&A, 507, 795
Walsh, A. J., Burton, M. G., Hyland, A. R., & Robinson, G. 1998, MNRAS, 301, 640
van der Walt, D. J., Churchwell, E., Gaylard, M. J., & Goedhart, S. 2003, MNRAS, 341, 270
van der Walt, D. J., Sobolev, A. M., & Butner, H. 2007, A&A, 464, 1015
Xu, Y., Li, J. J., Hachisuka, K., et al. 2008, A&A, 485, 729